Bol. Soc. Paran. Mat.
©SPM – E-ISSN-2175-1188
SPM: www.spm.uem.br/bspm

(3s.) **v. 2026 (44) 2** : 1–16.
ISSN-0037-8712
doi:10.5269/bspm.80577

Hall Current and Ion Slip Effects on Three-Dimensional Radiating Eyring-Powell Fluid Flow Past a Stretching Sheet with Prandtl Number and Magnetic Field

M. V. Phani Kumari[1], Ch. Siva Subrahmanyam[2], S. Jana Reddy[3] and R. Srinivasa Raju[4]

ABSTRACT: This work determines the effect of ion slip and Hall current on the three-dimensional Eyring-Powell fluid flow across a stretched sheet by considering the Prandtl number, magnetic fields, and temperature radiation. With the use of MATLAB's "bvp4c" solution, the regulating equations may be reduced to a system of nonlinear ordinary differential equations. Main and secondary velocity patterns, temperature distributions, skin-friction coefficients, and Nusselt number are examined using a variety of non-numerical parameters. To validate the numerical technique, previous research was compared to it. Results demonstrate strong agreement, indicating the analysis was accurate and dependable. One noticeable effect of the magnetic field parameter is a much smaller velocity boundary layer. When the Eyring-Powell factors modify the velocity, the observed findings are seen to be incorrect. In general, a lower Prandtl-Biot number indicates decreasing temperatures and a greater thermophoretic while Brownian motion coefficient indicates increasing temperatures. We examine the three-dimensional effects of heat radiation, Hall current, and ion slips on the flow of a Casson nanofluid using computational approaches for a stretched sheet. A solution to the governing equations is found using MATLAB's bvp4c function. In our knowledge, no previous studies have investigated the combination of physical effects with modeling techniques in this way.

Keywords: Hall current, three-dimensional, Erying-Powell fluid, MHD, hall current, ion slip.

Contents

Nomenclature

List of Symbols

$u_w\,(x)$**:** Stretching velocity of the fluid along x - direction (m/s)
$x,\ y,\ z$**:** Cartesian coordinates measured along the stretching sheet (m)
$v_w\,(y)$: Stretching velocity of the fluid along y - direction (m/s)
$u,\ v,\ w$**:** Velocity components in x, y and z axes respectively (m/s)
f**:** Dimensionless stream function along x - direction $(kg\ /\ m.\ s)$
$a,\ b$**:** Constants
g**:** Dimensionless stream function along y - direction $(kg\ /\ m.\ s)$
f'**:** Fluid velocity along x – direction (m/s)
g'**:** Fluid velocity along y – direction (m/s)
q_w**:** Heat flux coefficient
M^2**:** Magnetic field parameter
Nu**:** Rate of heat transfer coefficient
Re_x**:** Reynolds number along x - direction

2020 *Mathematics Subject Classification:* 76W05, 76D05, 78A40.
Submitted December 04, 2025. Published March 14, 2026

Re_y**:** Reynolds number along y - direction
Cfx**:** Skin-friction coefficient along x - direction (s^{-1})
Cfy**:** Skin-friction coefficient along y - direction (s^{-1})
C_p**:** Specific heat capacity of nano particles $(J\ /\ kg\ /\ K)$
T_w**:** Temperature at the surface (K)
T_∞**:** Temperature of the fluid far away from the stretching sheet (K)
B_o**:** Uniform magnetic field $(Tesla)$
Pr**:** Prandtl number
T**:** Fluid temperature (K)
B: Magnetic field vector
p**:** Pressure
I**:** Identity tensor
C**:** Characteristics of Erying-Powell fluid
Nr **:** Thermal radiation parameter
q_r**:** Radiative heat flux
J: Current density vector
J_x, J_z: Components of Current density vector
K^*: Rosseland mean absorption coefficient
E: Electric field's intensity vector
V: Velocity vector

Greek symbols:

μ**:** Dynamic viscosity of the fluid
ε**:** Erying-Powell fluid parameter
η**:** Dimensionless similarity variable (m)
θ**:** Dimensionless temperature (K)
σ**:** Electrical Conductivity
σ^***:** Stefan Boltzmann constant
ρ**:** Fluid density $(kg\ /\ m^3)$
ν**:** Kinematic viscosity $(m^2\ /\ s)$
κ**:** Thermal conductivity of the fluid
α**:** Thermal diffusivity, $(m^2\ /\ s)$
τ_1**:** Parameter defined as $\left(\frac{(\rho C)_p}{(\rho C)_f}\right)$
τ**:** Cauchy stress tensor
τ_{wx}**:** Wall shear stress along x - direction
τ_{wy}**:** Wall shear stress along y – direction
δ_1, δ_2**:** Fluid parameters
ψ: Stream function
m**:** Hall parameter
β_i**:** Ion Slip parameter
β_e**:** Hall current parameter
ω_e**:** Cyclotron frequency
τ_e**:** Electrical collision time
δ: Stretching ratio parameter

Superscript:

$'$: Differentiation w.r.t η

Subscripts:

f**:** Fluid
w**:** Condition on the sheet
∞**:** Ambient Conditions

1. Introduction

Hall and ion slip effects in magnetohydrodynamic fluxes are expanding in significance due to their substantial impact on flow behavior. When charged particles and magnetic fields interact, they produce electric fields in their orbital. The name for the phenomena we just discussed is called the Hall effect. Thanks to the ion slip effect, charged particles travel at a different speed than the neutral stream. Because these effects may alter the mechanism of flow and the rate of heat transfer, studying them is crucial for improving magnetohydrodynamic (MHD) fluxes. Strong electromagnetic forces, manifested in high magnetic fields, amplify the Hall current and ion-slip effects. Lots of scientists are now trying to figure out the function of Hall currents and ion leakage. After considering the impacts of ion slip and Hall current, Akram et al. [1] investigated the behavior of a two-phase model in a radiative non-Newtonian nanofluid flow. What effects do ion leaks and Hall current have on the flow of hybrid nanofluid as it passes over a two-way stretched surface? Alharbi et al. [2] investigated these questions. Studying the effects of gyrotactic microorganisms and changing characteristics on the flow of a three-dimensional Maxwell nanofluid across a rotating plate, Ali and colleagues [3] investigated the role of ion slip and Hall current. How Hall and ion-slip currents impact the thermal characteristics of magnetic power-law hybrid nanofluids was investigated in a work by Sultana et al. [4] using a modified version of Fourier's law. The movement of heat and mass through second-grade, diffuse materials is a topic of interest for micromachines, and Deepthi and colleagues [5] developed a model to explain this phenomenon. Internal processes such as thermodiffusion, ion slip, and the Hall effect are included into the model. Examining the effects of chemical processes, Cattaneo-Christov heat flow, ion slip, Hall current, and ternary hybrid nanofluid flow across a two-way surface was the focus of Gul et al. [6]. Investigating the effects of radiation absorption, Hall current, and ion-slip current on magnetohydrodynamic convection, Rajakumar et al. [7] investigated temperature variations dispersed in a sine wave form. Mehmood et al. investigated the impact of ion-slip and Hall current effects on the heat transfer mechanisms in viscoelastic flow via a porous elastic membrane in their research [8]. An investigation of the settling of thermophoretic particles in a double-diffusive Ree-Eyring fluid flow between two flexible spinning disks was carried out by Li et al. [9]. Impacts of ion slip and Hall current were examined. Das and colleagues investigated the effects of ion-slip and Hall currents on the flow of magneton nanofluids in a channel with variable porosity in their research [10]. Simulating the impacts of Hall current and ion slip, Ramzan and colleagues investigated the impact of microorganisms in motion on the flow of Sutterby nanofluid over a rotating disk [11]. Utilizing computational techniques, Anwar Bég et al. [12] investigated unstable nonlinear magnetohydrodynamic micropolar transport phenomena, including Hall and ion-slip currents. Researchers Islam and colleagues [13] investigated the effects of ion-slip and Hall currents on fluid flow inside a curved, rotating square duct subjected to a magnetic field. Hall and ion slip were investigated by Akbar et al. [14] in a three-dimensional Prandtl model with generalized mass and heat fluxes and an entropy analysis. The impact of Hall and ion slip on the flow of hybrid nanoparticles (Au-GO/blood) was investigated by Khanduri and colleagues using a catheterized artery that was both stenosed and clotted [15]. Research by Nasrin et al. [16] examined ion drift and Hall effects in a Couette flow that was unstable and situated between two horizontal Riga plates. Using a peristaltic-wave endoscope, Das et al. [17] investigated the effects of Hall and ion slip currents on the magnetohydrodynamic blood flow of mixed nanoparticles. In a peristaltic microchannel, Das and colleagues [18] investigated the Hall and ion-slip current effects on the electro-osmotic flow of an ionic hybrid nanofluid. The unusual magnetohydrodynamic flow of a second-grade fluid in a porous media was investigated by Raghunath et al. [19]. Various effects on the flow were examined, including ion slip, radiation absorption, diffusion thermoelectricity, and the Hall effect. In their study, Scientists Das and colleagues et al. [20] used electroosmosis and peristaltic processes to study the flow of an ionic Casson hybrid nanofluid via microchannels and the impacts of Hall and ion-slip currents.

We want to find out what happens when an immobile, thick, electrically conducting Erying-Powell fluid is close to a stretching sheet. We will look at how Hall current, ion leaks, magnetic field, and heat radiation affect it. This numerical method uses the "bvp4c" tool in MATLAB to break down the governing equations and solve them over and over again, producing numerical answers. This study will look at how different factors affect the rates of heat and momentum transfer on the surface. This will help figure out how important physical factors affect temperature and primary and secondary velocity patterns. This study aims to fill in a gap in our knowledge by collecting useful information that will help

make flow scenario design and optimization better.

2. Mathematical Modelling

The effect of heat radiation, Hall current, and ion leakage on a three-dimensional Eyring-Powell fluid flowing across a stretched sheet devoid of electrical current was examined in this work. A magnetic field is applied to the liquid. You can see the coordinate system utilized for this fluid flow issue in Figure 1. A few assertions about this project are detailed below.

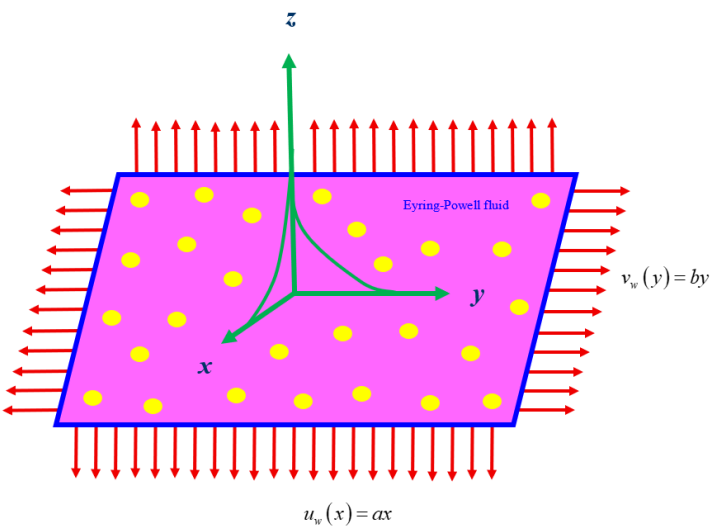

Figure 1: Geometrical representation of Eyring-Powell fluid flow

a) An electric current flows through a fluid as a magnetic field ($B = 0, 0, B_0$) is applied along the z-axis.

b) If the magnetic Reynolds number is small, then the produced magnetic field is ignored.

c) The vectors u, v, and w represent the x-, y-, and z-direction components of a motion, respectively.

d) An exponential growth rate of the surface causes induced flow.

e) Therefore, potential energy and concentration calculations do not account for the Soret and Dufour effects.

f) Joule heating and viscous loss are ignored in the energy calculation.

g) Concentration measurements do not make use of chemical procedures.

h) The description of the border circumstances is lacking in its emphasis on the many slip consequences.

i) Neither thermophoresis nor Brownian motion are included in the energy calculation for nanofluid mobility.

j) In consideration of Hall current and ion sliding in the momentum equations.

k) The Cauchy stress tensor T describes an Eyring-Powell fluid and may be expressed as

$$T = -pI + \tau \tag{2.1}$$

$$\rho a_i = -\nabla p + \nabla.(\tau_{ij}) + \sigma J \times B \tag{2.2}$$

Within the framework of an Eyring-Powell fluid model, τ_{ij}may also represent

$$\tau_{ij} = \mu\left(\frac{\partial u_i}{\partial x_j}\right) + \frac{1}{\varepsilon}\sinh^{-1}\left(\frac{1}{c}.\frac{\partial u_i}{\partial x_j}\right) \tag{2.3}$$

Here, we have the identity vector (I), pressure (p), and qualities of the Eyring-Powell fluid (ε and c). Deciding to

$$\sinh^{-1}\left(\frac{1}{c}\times\frac{\partial u_i}{\partial x_j}\right) \cong \frac{1}{c}\times\frac{\partial u_i}{\partial x_j} - \frac{1}{6}\left(\frac{1}{c}\times\frac{\partial u_i}{\partial x_j}\right)^3, \quad \left|\frac{1}{c}\times\frac{\partial u_i}{\partial x_j}\right| \prec 1 \tag{2.4}$$

l) Here is the revised generalized formula for Ohm's law, applicable to very powerful magnetic fields:

$$J = \sigma\left[E + (V\times B)\right] - \frac{\omega_e\tau_e}{B_o}(J\times B) + \frac{\omega_e\tau_e\beta_i}{B_o^2}\left[(J\times B)\times B\right] \tag{2.5}$$

m) Simultaneously, Eq. (2.5) is simplified to

$$J_x = (\sigma B_o)\times\left[\frac{\beta_e u - (1+\beta_e\beta_i)\,w}{(1+\beta_e\beta_i)^2+\beta_e^2}\right] \& J_z = (\sigma B_o)\times\left[\frac{(1+\beta_e\beta_i)\,u + \beta_e w}{(1+\beta_e\beta_i)^2+\beta_e^2}\right] \tag{2.6}$$

n) Radiative heat flow is defined as follows by the Roseland estimate:

$$q_r = -\frac{4\sigma^*}{3K^*}\left(\frac{\partial T^4}{\partial z}\right) \tag{2.7}$$

One possible interpretation is that the T^4term may be generally expressed as a linear function of temperature if the temperature variations within the flow are large enough. This is accomplished by expanding T^4 with respect to the open stream temperature T_∞ using a Taylor series, as seen below:

$$T^4 = T_\infty^4 + 4T_\infty^3(T-T_\infty) + 6T_\infty^2(T-T_\infty)^2 + \ldots \tag{2.8}$$

After neglecting higher-order terms in the above equation beyond the first-degree term in $(T-T_\infty)$, we get
This is what we get when we remove the first-order term from the preceding equation involving $(T-T_\infty)$:

$$T^4 \cong 4T_\infty^3 T - 3T_\infty^4 \tag{2.9}$$

Therefore, by sub. Eq.(2.9) into Eq.(2.7), we get.

$$q_r = -\frac{16T_\infty^3\sigma^*}{3K^*}\left(\frac{\partial T}{\partial z}\right) \tag{2.10}$$

The fundamental governing equations, continuity, momentum, energy, concentration by applying the boundary layer approximations are

$$\frac{\partial u}{\partial x} + \frac{\partial v}{\partial y} + \frac{\partial w}{\partial z} = 0. \tag{2.11}$$

$$u\times\left(\frac{\partial u}{\partial x}\right) + v\times\left(\frac{\partial u}{\partial y}\right) + w\times\left(\frac{\partial u}{\partial z}\right) = \nu\times\left\{\left(\nu+\frac{1}{\rho\varepsilon C}\right) - \frac{1}{2\rho\varepsilon C^3}\left[\frac{\partial u}{\partial z}\right]^2\right\}$$
$$\times\left(\frac{\partial^2 u}{\partial z^2}\right) - \left(\frac{\sigma B_o^2}{\rho}\right)\left[\frac{(1+\beta_e\beta_i)\,u+\beta_e w}{(1+\beta_e\beta_i)^2+\beta_e^2}\right] \tag{2.12}$$

$$u\times\left(\frac{\partial v}{\partial x}\right)+v\times\left(\frac{\partial v}{\partial y}\right)+w\times\left(\frac{\partial v}{\partial z}\right)=\nu\times\left\{\left(\nu+\frac{1}{\rho\varepsilon C}\right)-\frac{1}{2\rho\varepsilon C^{3}}\left[\frac{\partial v}{\partial z}\right]^{2}\right\}\times\left(\frac{\partial^{2}v}{\partial z^{2}}\right)-\left(\frac{\sigma B_{o}^{2}}{\rho}\right)\left[\frac{\beta_{e}u-\left(1+\beta_{e}\beta_{i}\right)w}{\left(1+\beta_{e}\beta_{i}\right)^{2}+\beta_{e}^{2}}\right] \tag{2.13}$$

$$u\times\left(\frac{\partial T}{\partial x}\right)+v\times\left(\frac{\partial T}{\partial y}\right)+w\times\left(\frac{\partial T}{\partial z}\right)=\alpha\times\left(\frac{\partial^{2}T}{\partial z^{2}}\right)+\frac{1}{\rho C_{p}}\times\left(\frac{16T_{\infty}^{3}\sigma^{*}}{3K^{*}}\right)\times\left(\frac{\partial^{2}T}{\partial z^{2}}\right) \tag{2.14}$$

The boundary conditions for this flow are

$$\left.\begin{array}{l}u=u_{w}\left(x\right)=a\times x,\ \ v=v_{w}\left(y\right)=b\times y,\ \ w=0,\ \ T=T_{w},\ at\ \ z=0\\ u\to 0,\ \ v\to 0,\ \ T\to T_{\infty},\ as\ \ z\to\infty\end{array}\right\} \tag{2.15}$$

Presenting the subsequent changes of similarity

$$\left.\begin{array}{l}u=ax\times f'\left(\eta\right),\ v=by\times g'\left(\eta\right),\ w=-\sqrt{a\nu}\times\left\{f\left(\eta\right)+g\left(\eta\right)\right\},\\ \eta=\left(\sqrt{\frac{a}{\nu}}\right)\times z,\ \theta=\frac{T-T_{\infty}}{T_{w}-T_{\infty}},\ u=\frac{\partial\psi}{\partial y},\ v=-\frac{\partial\psi}{\partial x},.\end{array}\right\} \tag{2.16}$$

Making use of Eq. (2.16), Eqs. (2.12), (2.13), (2.14), take the following form

$$\left(1+\varepsilon\right)\times f'''-\varepsilon\delta_{1}f'''\times f''^{2}+f\times f''+g\times f''-f'^{2}-M^{2}\left[\frac{\left(1+\beta_{e}\beta_{i}\right)f'+\beta_{e}\times g'}{\left(1+\beta_{e}\beta_{i}\right)^{2}+\beta_{e}^{2}}\right]=0 \tag{2.17}$$

$$\left(1+\varepsilon\right)\times g'''-\varepsilon\delta_{2}g'''g''^{2}+g\times g''+f\times g''-g'^{2}-M^{2}\times\left[\frac{\beta_{e}f'-\left(1+\beta_{e}\beta_{i}\right)g'}{\left(1+\beta_{e}\beta_{i}\right)^{2}+\beta_{e}^{2}}\right]=0 \tag{2.18}$$

$$\left(1+\frac{4}{3Nr}\right)\theta''+\Pr f\theta'+\Pr g\theta'=0 \tag{2.19}$$

the corresponding boundary conditions (2.15) becomes

$$\left.\begin{array}{l}f\left(0\right)=0,\ g\left(0\right)=0,\ f'\left(0\right)=1,\ \ g'\left(0\right)=\delta,\ \ \theta\left(0\right)=1,\\ f'\left(\infty\right)\to 0,\ \ g'\left(\infty\right)\to 0,\ \ \theta\left(\infty\right)\to 0\end{array}\right\} \tag{2.20}$$

where the involved physical parameters are defined as

$$\left.M^{2}=\frac{\sigma B_{o}^{2}}{\rho a},\Pr=\frac{\nu}{\alpha},\delta=\frac{b}{a},Nr=\frac{\kappa K^{*}}{4\sigma^{*}T_{\infty}^{3}},\varepsilon=\frac{1}{\mu\beta C},\delta_{1}=\frac{a^{3}x^{2}}{2\nu C^{2}},\delta_{2}=\frac{a^{3}y^{2}}{2\nu C^{2}}\right\} \tag{2.21}$$

Down below, you can see the critical physical parameters, such as the x- and y-components of the skin-friction coefficient and the local Nusselt number:

$$Cfx=C_{f}\left(\sqrt{Re_{x}}\right)=\frac{\tau_{wx}}{\rho u_{w}^{2}}=\left\{\left(1+\varepsilon\right)f''\left(0\right)-\frac{1}{3}\varepsilon\delta_{1}f''^{3}\left(0\right)\right\} \tag{2.22}$$

$$Cfy=C_{f}\left(\sqrt{Re_{y}}\right)=\frac{\tau_{wy}}{\rho v_{w}^{2}}=\left\{\left(1+\varepsilon\right)g''\left(0\right)-\frac{1}{3}\varepsilon\delta_{2}g''^{3}\left(0\right)\right\} \tag{2.23}$$

$$\begin{aligned}Nu&=\frac{xq_{w}}{\kappa\left(T_{w}-T_{\infty}\right)}\\ \text{where } q_{w}&=-\kappa\left(\frac{\partial T}{\partial y}\right)_{y=0}+\left(q_{r}\right)_{w}\\ \Rightarrow Nu&=-\left(\sqrt{Re_{x}}\right)\left(1+\frac{4}{3Nr}\right)\theta'\left(0\right)\end{aligned} \tag{2.24}$$

In this scenario, the local Reynolds numbers are denoted as $Re_{x}=\frac{u_{x}(x)x}{\nu}$ and $Re_{y}=\frac{v_{w}(y)y}{\nu}$. Their foundation is in the stretching velocities, $u_{w}(x)$ and $v_{w}(y)$.

3. Numerical Solution by MATLAB "bvp4c" Solver

Elements (2.17)-(2.19) illustrate nonlinear differential equations of higher order. To see the boundary conditions, look at Equation (2.20). To get the numerical solutions to these ordinary differential equations, we use the bvp4c technique, which is part of the MATLAB computer platform. Through a three-stage application of the Lobatto IIIA Runge-Kutta technique, the bvp4c algorithm achieves numerical results that are accurate to the fourth order. After all subsequent phases are completed, our physical model will include the bvp4c algorithm.

Step-1: A series of higher-order, non-linear ODE's are supplemented with additional variables in equations (2.17) through (2.19).

$$\left.\begin{array}{l} y(1)=f,\ y(2)=f',\ y(3)=f'',\ y(4)=g, \\ y(5)=g',\ y(6)=g'',\ y(7)=\theta,\ y(8)=\theta'. \end{array}\right\} \tag{3.1}$$

Step-2: Transform the system of higher-order, non-linear ODE's presented in Equations (2.19)–(2.23) into a system of identical 1^{st} order, nonlinear ordinary differential equations using the additional variables provided in Equation (3.1).

$$f''' = \frac{\left\{\begin{array}{l} -y(1)\times y(3) - y(4)\times y(3) + (y(2))^2 \\ +M^2\times y(2) + M^2\times\left[\frac{(1+\beta_e\beta_i)y(2)+\beta_e y(5)}{(1+\beta_e\beta_i)^2+\beta_e^2}\right] \end{array}\right\}}{\left\{(1+\varepsilon)-\varepsilon\delta_1\times(y(3))^2\right\}} \tag{3.2}$$

$$g''' = \frac{\left\{\begin{array}{l} -y(4)\,y(6) - y(1)\,y(6) + (y(5))^2 \\ +M^2 y(5) + M^2\left[\frac{\beta_e y(2)-(1+\beta_e\beta_i)y(5)}{(1+\beta_e\beta_i)^2+\beta_e^2}\right] \end{array}\right\}}{\left\{(1+\varepsilon)-\varepsilon\delta_2\,(y(6))^2\right\}} \tag{3.3}$$

$$\theta'' = \frac{\{-\Pr\times y(1)\times y(8) - \Pr\times y(4)\times y(8)\}}{\left\{1+\frac{4}{3Nr}\right\}} \tag{3.4}$$

Step-3: Plug the additional variables from Eq. (3.1), into Eq. (2.20), to get the boundary conditions.

$$\left.\begin{array}{llll} [y(1)]_p=0, & [y(4)]_p=0, & [y(2)]_p=1, & [y(5)]_p=\delta, \\ [y(7)]_p=1, & [y(2)]_q=0, & [y(5)]_q=0, & [y(7)]_q=0, \end{array}\right\} \tag{3.5}$$

The letters "p" and "q" show where the sheet is when $\eta=0$ and where it is when η is a certain number. In this research, this spot is set at $\eta=3$ for primary velocity profiles, $\eta=4$ for secondary velocity profiles, and $\eta=6$ for temperature, quantity, and microbe profiles.

Step-4: As a fourth phase, the set of boundary conditions (2.2) and the 1^{st} order, non-linear ODE's (3.2) through (3.4), are mathematically combined using the bvp4c solver.

Step-5: Make sure you use 2 sets of starting values sequentially when using the "bvp4c" method. This will provide the 1^{st} and subsequent solutions. The implementation of both primary and secondary concepts becomes more simpler as a result. Repeat this procedure with a fresh set of initial values until you get the results you want. If the expected patterns of velocity and temperature are consistent with Eq. (2.19), then the initial assumptions are believed to be true. I typically need to exert a lot of effort in order to get a decent first set of results. Initial impressions put together.

4. Code Validation

In order to compare their computed Nusselt number coefficients with those discovered by Hayat et al. [21], they excluded β_e and β_i and examined a variety of M, Pr, Nr, and ε values (refer to Table 1) to test for compatibility. The comparative findings in the table confirmed the accuracy and reliability of our computation approach, which is consistent with previous research.

Table 1: Assuming $\beta_e = \beta_i = 0$, the current Nusselt number coefficient values are contrasted with those provided by Hayat et al. [21].

M	Pr	Nr	ε	Hayat et al. [21] results	Present results
0.0	0.71	0.5	0.5	0.65496	0.6356905969
0.7				0.62357	0.6357871607
1.5				0.54949	0.5394695239
	1.0			0.59586	0.5788483873
	1.5			0.78096	0.7976723806
		1.0		0.41365	0.4038395911
		3.0		0.58315	0.5664545821
			0.7	0.57725	0.5777160818
			1.5	0.61980	0.6023464925

5. Results and Discussion

The objective of pictures 2-12 is to examine the characteristics of main and subordinate non-dimensional motion and temperature patterns across several developmental parameters, including the variables that are considered include the Prandtl number (Pr), the heat radiation (Nr), the ion slip (β_e), the stretching sheet (δ), the Hall current (β_i), and the magnetic field (M^2). Two engineering parameters skin friction coefficients and heat transfer rate coefficients are shown in Tables 2 and 3, respectively, based on the main and secondary velocity profiles. These values match to several developmental parameters previously referenced. It is essential to recognize that, unless indicated differently in the graphs, the default parameter values used in the study were: $M^2 = 0.1$, $\varepsilon = 0.2$, $\delta_1 = 0.2$, $\delta_2 = 0.3$, $\beta_e = 0.3$, $\beta_i = 0.2$, $\delta = 0.5$, $Nr = 0.5$, and Pr $= 0.71$.

- Increasing the magnetic field parameter narrows the boundary layer thickness and reduces the amplitudes of the main and subordinate velocity curves, as seen in Figures 2 and 3. What is occurring right now is the consequence of a magnetic field acting upon a sensitive fluid while an electric current flows through it. Drag reduces the velocity of liquids moving through the boundary layer. At that point, magnetic fields have no more value.

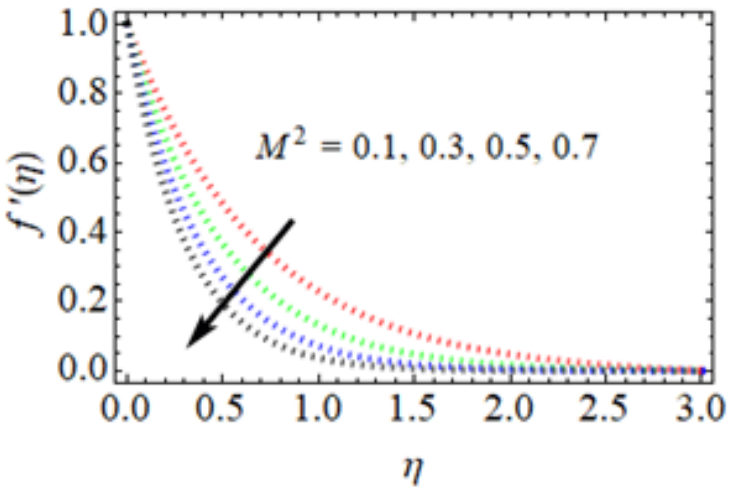

Figure 2: The primary velocity profiles for different values of M^2.

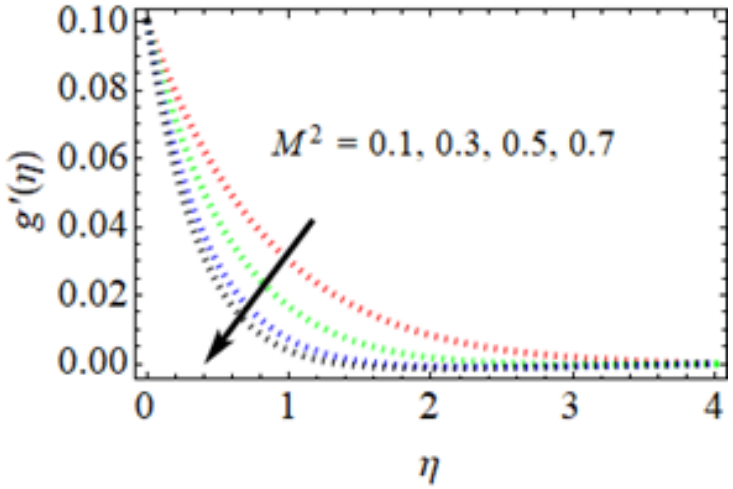

Figure 3: The secondary velocity profiles for different values of M^2.

- Pictured in Figures 4 and 5, this demonstrates the primary and secondary velocity patterns of an Eyring-Powell fluid. It was discovered that greater values of the Eyring-Powell fluid parameters were closely associated with higher velocity rates.

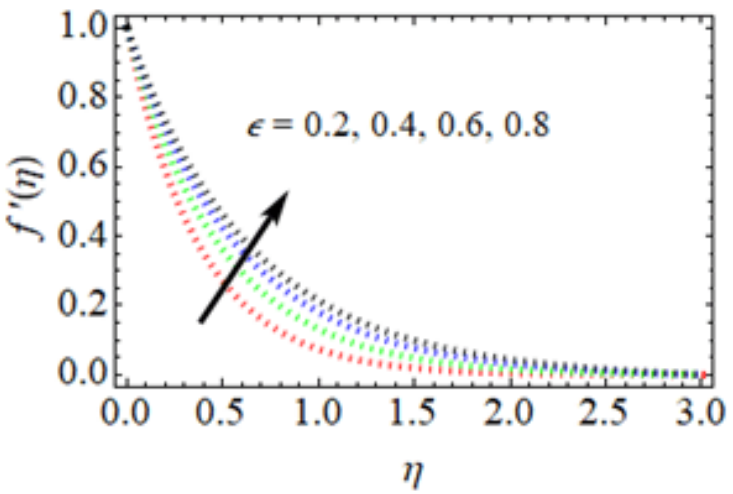

Figure 4: The primary velocity profiles for different values of ε.

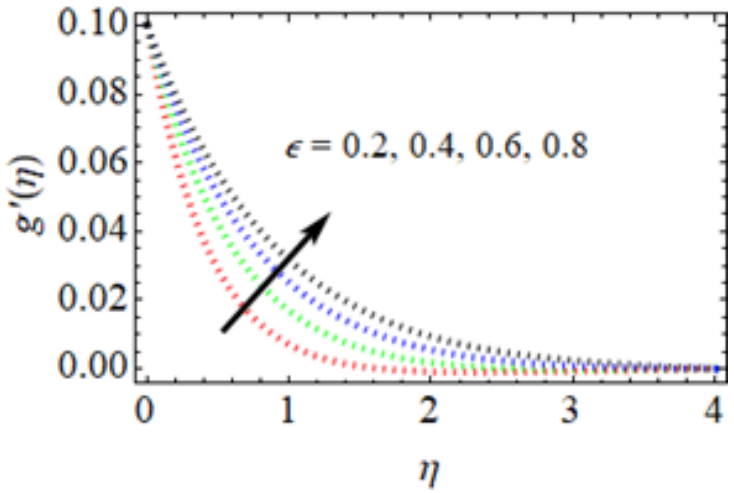

Figure 5: The secondary velocity profiles for different values of ε.

- Figures 6 and 7 show that the velocity patterns of the main and secondary components are changed by the Hall parameter (β_e). Reduced effective electrical conductivity due to the Hall constant results in a smaller magnetic resistance Lorentz force. Both the main and secondary velocities increased as a result of the enhanced fluid dynamics seen in Figures 6 and 7.

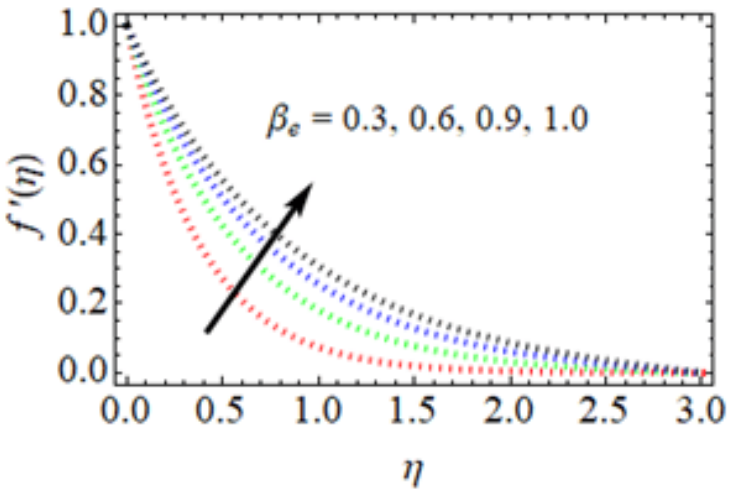

Figure 6: The primary velocity profiles for different values of βe.

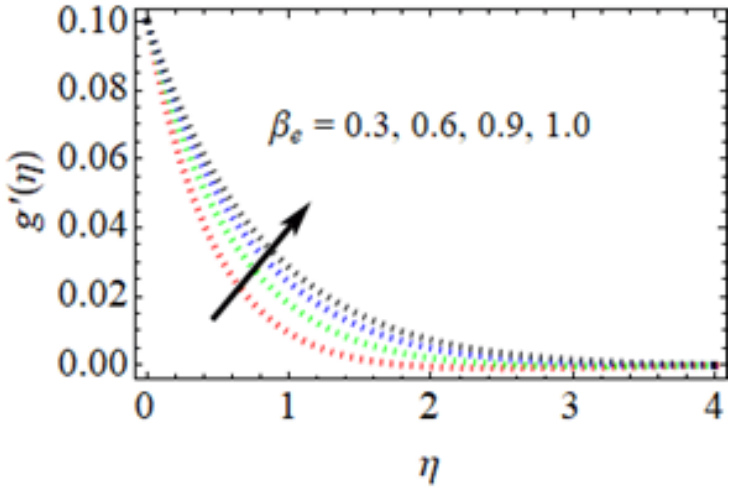

Figure 7: The secondary velocity profiles for different values of βe.

- It's clear from Figures 8 and 9 how the ion loss measure (β_i) impacts things. Greater values of the ion slip parameter result in a weaker retarding or slowing force. Attenuating the delay causes an growth in both the main and subordinate velocity curves.

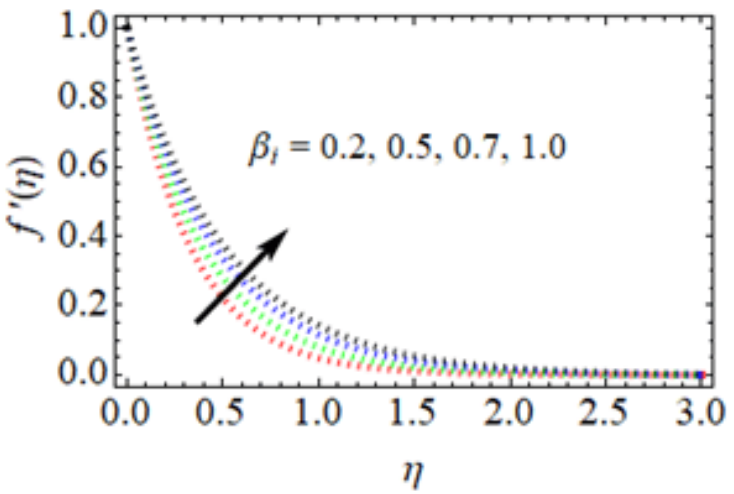

Figure 8: The primary velocity profiles for different values of βi.

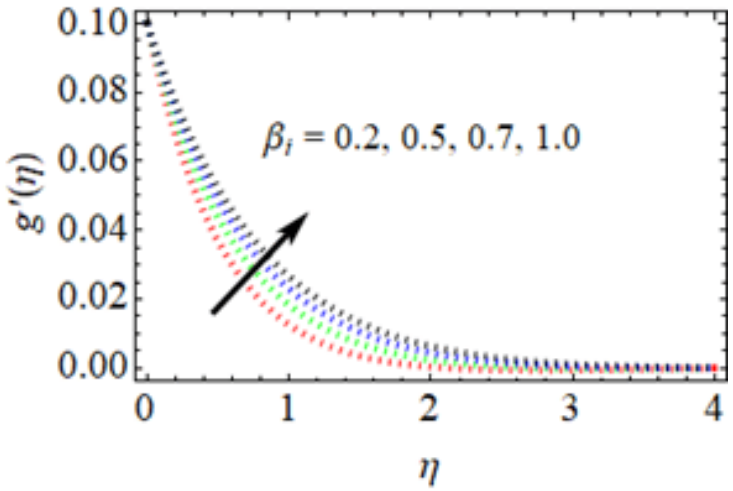

Figure 9: The secondary velocity profiles for different values of βi.

- You can see the effects of the stretching ratio on the secondary velocity curve in Figure 10. Higher values for the stretching rate ratio are accompanied with higher secondary velocity curves. The strain measurement and the flow pressure often both increase simultaneously.

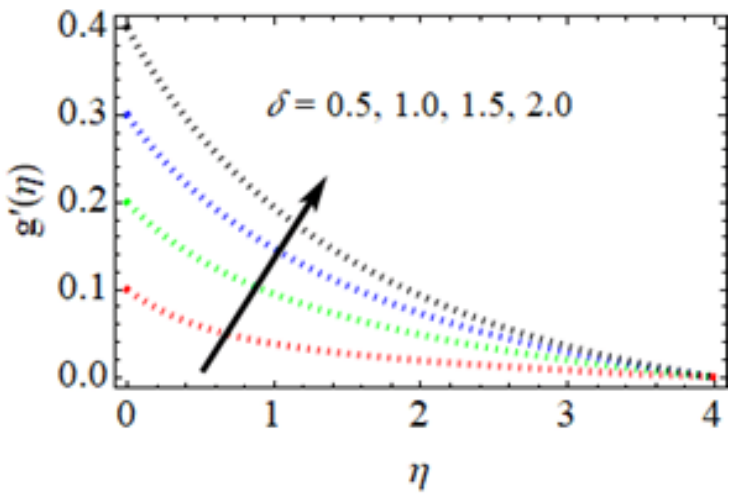

Figure 10: The secondary velocity profiles for different values of δ.

- These fluid parameters, including temperature and Prandtl number, are shown in Figure 11. By raising the Prandtl number, the temperature gradient that the fluid is able to perceive is reduced. Just because heat can't flow through fluids with a higher Prandtl value doesn't mean they're hotter.

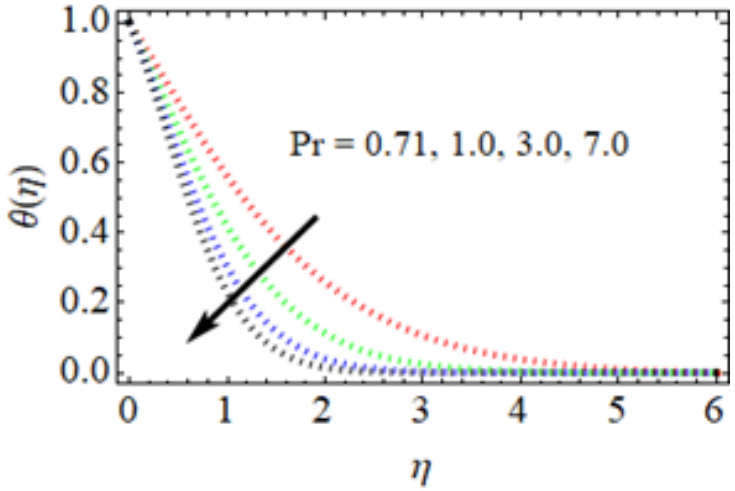

Figure 11: The temperature profiles for different values of Pr.

- You can see the patterns of temperature change in the thermal radiation measure Nr in this Figure 12. Reducing the temperature field is the result of raising the thermal radiation measure.

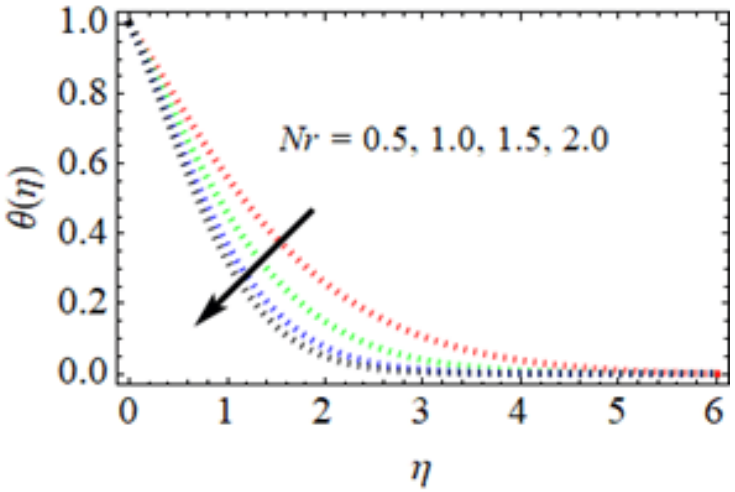

Figure 12: The temperature profiles for different values of Nr.

Table 2: Quantitative measurements of the skin-friction coefficient (Cfx)

M^2	ε	β_i	β_e	δ	Pr	Nr	Cfx
0.1	0.2	0.2	0.3	0.5	0.71	0.5	2.6646535822
0.3							2.6306576091
0.5							2.6020476273
	0.4						2.6863361741
	0.6						2.7104052815
		0.5					2.6920407853
		0.7					2.7270456357
			0.6				2.7025435974
			0.9				2.7351434792
				1.0			2.7027466034
				1.5			2.7456471999
					1.00		2.6256781728
					7.00		2.5914582562
						1.0	2.6395732579
						1.5	2.6164659154

- Details on the Skin-friction coefficients impacted by modifications to technical parameters may be found in Table 2. Among them, you can find the following parameters: the magnetic field (M^2), the Erying-Powell fluid (ε), the Hall current (β_i), the Ion Slip (β_e), the stretching sheet (δ), the Prandtl number (Pr), and the thermal radiation (Nr). The skin-friction coefficients increase when the following parameters are raised: the Erying-Powell fluid parameter (δ), the Hall current parameter (β_i), the ion slip parameter (β_e), and the stretching sheet parameter (ε). The magnetic field parameter (M^2), the Prandtl number (Pr), and the thermal radiation parameter (Nr) all decrease when their values are increased.

Table 3: Ratios of heat transfer rates expressed numerically

Pr	Nr	Nu
0.71	0.5	1.9154825484
1.00		1.8737848751
7.00		1.8504582058
	1.0	1.8848660963
	1.5	1.8534249479

- In addition to the Prandtl numbers (Pr), the Nusselt number (Nr), and the heat transfer rate (Pr), which might fluctuate, are shown in Table 3. According to the data in the table, with increasing Pr and Nr, the heat transfer coefficient decreases.

6. Conclusions

A three-dimensional, radiating, noncompressible, viscous, electrically conducting Powell-Erying fluid is in a continual state of motion over an extended sheet. Ion slip current and other Hall current phenomena, as well as the Prandtl number and heat radiation, are all factors in the flow. The most significant discoveries are listed below.

- One example is that, while the main and subordinate velocity curves shrink with growing magnetic field strength, they swell with growing values of the Hall parameter, the ion slip parameter, and the Powell-Erying fluid parameters.

- The spread of temperatures gets less even as the Prandtl number and Thermal radiation measure go up.

- The numbers found here are more accurate than the ones Hayat et al. [21] released, which didn't include β_e and β_i and used different values of M^2, Pr, Nr, and ε.

References

1. Akram, Mohammad, Osama Ala'yed, Rania Saadeh, Ahmad Qazza, A. M. Obalalu, Umair Khan, Adil Darvesh, A. A. Usman, A. M. Abdul-Yekeen, and Syed Modassir Hussain. "Exploring the dynamic behavior of the two-phase model in radiative non-Newtonian nanofluid flow with Hall current and ion slip effects." Journal of Radiation Research and Applied Sciences 17, no. 4 (2024): 101112.

2. Alharbi, Khalid Abdulkhaliq M., Maryam Afsar, Muhammad Ramzan, Nazia Shahmir, Seifedine Kadry, and Abdulkafi Mohammed Saeed. "Comparative study of hybrid nanofluid flows over a bidirectional stretched surface with the impact of Hall current and ion slip." Numerical Heat Transfer, Part A: Applications 85, no. 17 (2024): 2819-2835.

3. Ali, Jawad, Muhammad Ramzan, C. Ahamed Saleel, Seifedine Kadry, and Abdulkafi Mohammed Saeed. "Significance of Hall current and Ion slip in a three-dimensional Maxwell nanofluid flow over rotating disk with variable characteristics and gyrotactic microorganisms." Numerical Heat Transfer, Part B: Fundamentals 85, no. 5 (2024): 587-603.

4. Sultana, N., S. Shaw, S. Mondal, M. K. Nayak, S. Nazari, Abir Mouldi, and Ali J. Chamkha. "Hall and ion-slip current efficacy on thermal performance of magnetic power-law hybrid nanofluid using modified Fourier's law." Ain Shams Engineering Journal 15, no. 8 (2024): 102838.

5. Deepthi, V. V. L., Maha M. A. Lashin, N. Ravi Kumar, Kodi Raghunath, Farhan Ali, Mowffaq Oreijah, Kamel Guedri, El Sayed Mohamed Tag-ElDin, M. Ijaz Khan, and Ahmed M. Galal. "Recent development of heat and mass transport in the presence of Hall, ion slip and thermo diffusion in radiative second grade material: application of micromachines." Micromachines 13, no. 10 (2022): 1566.

6. Gul, Hina, Muhammad Ramzan, C. Ahamed Saleel, and Seifedine Kadry. "Hall current and ion slip effects on a ternary hybrid nanofluid flow over a bidirectional surface with chemical reaction and Cattaneo-Christov heat flux." Numerical Heat Transfer, Part A: Applications 86, no. 9 (2025): 2884-2899.

7. Rajakumar, K. V. B., N. Ranganath, T. Govinda Rao, and R. Srinivasa Raju. "Radiation absorption, Hall and ion-slip current-driven MHD convection with spanwise cosinusoidally fluctuating temperature: a perturbative study." Radiation Effects and Defects in Solids 180, no. 5-6 (2025): 661-695.

8. Mehmood, Rashid, Sehrish Khan, Ehnber Naheed Maraj, Shagufta Ijaz, and Siddra Rana. "Heat transport mechanism via ion-slip and Hall current in viscoplastic flow along a porous elastic sheet." Proceedings of the Institution of Mechanical Engineers, Part E: Journal of Process Mechanical Engineering 236, no. 3 (2022): 907-914.

9. Li, Shuguang, Naila Shaheen, Muhammad Ramzan, Seifedine Kadry, and C. Ahmad Saleel. "Thermophoretic particle deposition on double-diffusive Ree-Eyring fluid flow across two deformable rotating disks with Hall current and Ion slip." Journal of Magnetism and Magnetic Materials 589 (2024): 171547.

10. Das, S., B. Barman, and R. N. Jana. "Influence of Hall and ion-slip currents on peristaltic transport of magneto-nanofluid in an asymmetric channel." BioNanoScience 11, no. 3 (2021): 720-738.

11. Ramzan, Muhammad, Asad Ali Shah, Nazia Shahmir, Saad Alshahrani, and Seifedine Kadry. "Impact of motile microorganisms on a Sutterby nanofluid flow over a rotating disk with Hall current and ion slip." Numerical Heat Transfer, Part A: Applications 86, no. 13 (2025): 4537-4555.

12. Anwar Bég, Osman, Tasveer Anwara Bég, Mohammad Ferdows, Vasu Buddakkagari, Ali Kadir, Henry John Leonard, and Sireetorn Kuharat. "Unsteady nonlinear magnetohydrodynamic micropolar transport phenomena with Hall and Ion-slip current effects: Numerical study." International Journal of Applied Electromagnetics and Mechanics 65, no. 2 (2021): 371-403.

13. Islam, Md Rafiqul, Md Abdus Samad, and Md Mahmud Alam. "Hall and Ion-slip current effects on steady fluid flow through a rotating curved square duct with magnetic field." The European Physical Journal Plus 136, no. 12 (2021): 1204.

14. Akbar, Sana, Muhammad Sohail, Syed Tehseen Abbas, and Abha Singh. "Contribution of hall and ion slip effects with generalized mass and heat fluxes with entropy analysis on three-dimensional Prandtl model." Alexandria Engineering Journal 108 (2024): 244-260.

15. Khanduri, Umesh, and Bhupendra Kumar Sharma. "Hall and ion slip effects on hybrid nanoparticles (Au-GO/blood) flow through a catheterized stenosed artery with thrombosis." Proceedings of the Institution of Mechanical Engineers, Part C: Journal of Mechanical Engineering Science 237, no. 10 (2023): 2256-2278.

16. Nasrin, S., R. N. Mondal, and M. M. Alam. "Unsteady Couette flow past between two horizontal Riga plates with hall and ion slip effects." Math. Stat. 9, no. 4 (2021): 552-565.

17. Das, S., B. Barman, R. N. Jana, and O. D. Makinde. "Hall and ion slip currents' impact on electromagnetic blood flow conveying hybrid nanoparticles through an endoscope with peristaltic waves." BioNanoScience 11, no. 3 (2021): 770-792.

18. Das, Sanatan, and B. Barman. "Ramification of hall and ion-slip currents on electro-osmosis of ionic hybrid nanofluid in a peristaltic microchannel." BioNanoScience 12, no. 3 (2022): 957-978.

19. Raghunath, Kodi, Ravuri Mohana Ramana, Charankumar Ganteda, Prem Kumar Chaurasiya, Damodar Tiwari, Rajan Kumar, Dharam Buddhi, and Kuldeep Kumar Saxena. "Processing to pass unsteady MHD flow of a second-grade fluid through a porous medium in the presence of radiation absorption exhibits Diffusion thermo, hall and ion slip effects." Advances in Materials and Processing Technologies 10, no. 2 (2024): 754-771.

20. Das, Sanatan, Bhola Nath Barman, and Rabindra Nath Jana. "Hall and ion-slip currents' role in transportation dynamics of ionic Casson hybrid nano-liquid in a microchannel via electroosmosis and peristalsis." Korea-Australia Rheology Journal 33, no. 4 (2021): 367-391.

21. T. Hayat, M. Awais, S. Asghar, Radiative effects in a three-dimensional flow of MHD Eyring-Powell fluid, J. Egyptian Mathematical Society (2013) 21, pp. 379-384.

[1] *Department of Mathematics, Geethanjali College of Engineering, Keesara Mandal, Cheeryal Village, Hyderabad, Telangana, 501303, India.*

and

[2] *Department of Mathematics, NRI Institute of Technology, Agiripalli, Eluru (Dt), 521211, Andhra Pradesh, India.*

and

[3] *Department of H&S, KG Reddy College of Engineering and Technology, Chilkur, Moinabad, Hyderabad, 500075, Telangana State, India.*

and

[4] *Department of Mathematics and Statistics, GITAM (Deemed to be University), Hyderabad campus, Rudraram, Sangareddy (Dt), 502329, Telangana State, India.*
E-mail address: drallaba@gitam.edu